THESIS FOR THE DEGREE OF DOCTOR OF PHILOSOPHY IN SOLID AND STRUCTURAL MECHANICS

Material Modelling of Adipose Tissue for Traffic Injury Prevention

A Finite Element Study of Parameters Influencing Lap Belt to Pelvis Interaction

HOSEIN NASERI

Department of Mechanics and Maritime Sciences
CHALMERS UNIVERSITY OF TECHNOLOGY
Göteborg, Sweden 2020

Material Modelling of Adipose Tissue for Traffic Injury Prevention
A Finite Element Study of Parameters Influencing Lap Belt to Pelvis Interaction
HOSEIN NASERI
ISBN 978-91-7905-254-6

© HOSEIN NASERI, 2020

Doktorsavhandlingar vid Chalmers tekniska högskola
Ny serie nr. 4721
ISSN 0346-718X
Department of Mechanics and Maritime Sciences
Chalmers University of Technology
SE-412 96 Göteborg
Sweden
Telephone: +46 (0)31-772 1000

Chalmers Reproservice
Göteborg, Sweden 2020

Material Modelling of Adipose Tissue for Traffic Injury Prevention
A Finite Element Study of Parameters Influencing Lap Belt to Pelvis Interaction
Thesis for the degree of Doctor of Philosophy in Solid and Structural Mechanics
HOSEIN NASERI
Department of Mechanics and Maritime Sciences
Chalmers University of Technology

Abstract

Traffic injury is one of the main reasons for traumatic injuries. Obese occupants are among the vulnerable populations with a higher risk of death and severe injuries. Notably, obesity is associated with a thick layer of subcutaneous adipose (fat) tissue. In case of a crash, this may influence how the lap belt engages with the pelvis resulting in submarining, i.e., the lap belt slipping over the iliac crest of the pelvis, causing severe injuries. A popular numerical method to study occupant injuries in motor-vehicle collisions involves using Finite Element Human Body Models (FEHBMs). However, current FEHBMs, such as the THUMS or GHBMC models, do not represent the obese population in body shape or material properties, and are unable to represent the submarining phenomenon. In particular, there is no appropriate constitutive model for adipose tissue in the FEHBMs, while the mechanical property of adipose tissue is important in the simulation of interaction between the human body and restraint systems or the impact with interior objects.

The first aim of this research was to establish a biofidelic constitutive model for adipose tissue mechanical response, at high strain rates and large deformations. For this purpose, a nonlinear viscoelastic constitutive model was formulated. Global sensitivity analysis was used as a tool to learn what mechanical properties of adipose tissue are identifiable from different test setups. Thus, a frequency-sweep test and a ramp loading-unloading shear test were applied to account for the adipose tissue behaviour at high strain rates and large deformations, respectively. The second aim was to identify which parameters influence submarining the most. It was found that the incompressibility (Poisson's ratio) of adipose tissue is the most important material parameter. With regard to safety design, important parameters include lap belt angle and pelvis rotation. Due to a thicker layer of adipose tissue, the effect of these parameters becomes more important for obese occupants, resulting in a higher risk of submarining. These findings support the development of biofidelic FEHBMs, as well as suitable restraint system designs in order to reduce the risk of submarining.

Keywords: Adipose tissue, Constitutive modelling, Finite element human body models, Global sensitivity analysis , Obesity, Submarining

to my beloved family

Preface

The work presented in this thesis has been started on February 2015 to March 2020 at the Division of Dynamics and the Division of Vehicle Safety at Mechanics and Maritime Sciences Department, Chalmers University of Technology. This project is financed through the Swedish Research Council (VR), grant no. 621-2013-3909, also received funding from the European Union's Horizon 2020 research and innovation program (the OSCCAR project), grant No. 768947, which are gratefully acknowledged.

First of all, I express my deepest gratitude to my main supervisor, Prof. Håkan Johansson for the invaluable guidance, kindness and support he has provided through these years. His constant encouragement, creative ideas and personal discipline were the main sources helping me to overcome challenging circumstances, the reason why he is my best teacher. I have learned a lot from all of instructive discussions we have had.

I would like to also thank my first co-supervisor, Karin Brolin for all of insight she gave me into impact biomechanics and human body modelling. To have meeting and discussion with her was never boring because of her energy and passion in the field of biomechanics. It was pity she had to leave the project in the middle of my PhD, but I was super lucky having Johan Iraeus replacing her as my supervisor. He is supportive, friendly and keen with an excellent engineering view in vehicle safety and injury prevention. Without Johan, this thesis would not be accomplished. I am indebted to him for all I have learned from him. I would like to also thank my colleagues and friends at Chalmers for creating a warm, pleasant and productive environment. Especially to Erik Brynskog, for the collaboration and support he provided in human body simulation.

Finally, I am grateful to my parents for their kindness and support. Especially, I like to thank my wonderful wife for her love, support and accompanying me in this journey. I am also thankful to my little son, Ali, for bringing much joy and happiness to my life. His arrival also made me to think and appreciate more the Chalmers vision; **Chalmers for a Sustainable Future**.

Gothenburg, March 2020
Hosein Naseri

Thesis

This thesis consists of an extended summary and the following appended papers:

Paper A Naseri H. and Johansson H. A Priori Assessment of Adipose Tissue Mechanical Testing by Global Sensitivity Analysis, *Journal of Biomechanical Engineering* 515 140 (5) (2018) 051008.

Paper B Naseri H., Johansson H., Brolin K., A Nonlinear Viscoelastic Model for Adipose Tissue Representing Tissue Response at a Wide Range of Strain Rates and High Strain Levels, *Journal of Biomechanical Engineering* 140 (4) (2018) 041009.

Paper C Naseri H., Iraeus J. and Johansson H., The Effect of Adipose Tissue Material Properties on the Lap Belt-Pelvis Interaction: A Global Sensitivity Analysis, Accepted for the publication in *Journal of the Mechanical Behvior of Biomedical Materials*.

Paper D Naseri H., Iraeus J. and Johansson H., A Numerical Study on the Risk of Lap Belt Submarining Considering Occupant and Vehicle Design Parameters, Submitted for international publication.

The appended papers were prepared in collaboration with the co-authors. The author of this thesis was responsible for the major progress of the work in preparing the papers, took part in developing the theory, performed all implementations and numerical calculations, and took part in writing the papers.

Contents

Part I
Extended Summary

1 Introduction

1.1 Motivation

Motor-vehicle injuries, also referred to as 'road-traffic injuries', are estimated to account for 1.25 million out of a total of 5 million fatal injuries worldwide [1]. The obese population is considered one of the vulnerable groups and the fatality risk in motor-vehicle collisions has been found to be increased for obese occupants in comparison to non-obese occupants [2]. Also, the increased risk of non-fatal injuries such as lower extremity, upper extremity and spine injuries have been associated with increased Body Mass Index (BMI) [3]. Further, studies [4, 5, 6, 7] on anthropometric measurements of seatbelt fit for different driver characteristics have found obesity to be one of the predominant reasons that the proper fit of seatbelts may be altered due to the routing of the seatbelt relative to the underlying skeletal structure displaced. In lap belt-pelvis interaction tests conducted on different Post Mortem Human Subjects (PMHSs), a lack of belt hooking by the pelvis was observed in cases where the soft tissue was too thick over the iliac crest [8]. A severe consequence of improper lap belt fit can be submarining. Submarining is defined as a situation where, in case of crash, the lap belt slips over the iliac crest of the pelvis, thereby influencing the kinematics of occupant response. The status of submarining in current real-world vehicle collisions is not known since it is difficult to determine submarining occurrence from real field data. However, submarining will most likely be of particular concern in future traffic safety with the arrival of self-driving cars [9] where it has been hypothesized that occupants will increasingly prefer travelling in a reclined position than in vehicles today. Field data studies [10] indicate that seatback recline angle increases severe injury and mortality rates. Computational analysis [11, 12] reported unfavourable occupant kinematics and submarining as a result of reclined seatback angle.

The precise mechanism giving rise to a higher risk of submarining, especially for obesity with a thicker layer of soft tissue, has not been well investigated. A traditional option for studying road-traffic injuries involves using Anthropomorphic Test Devices (ATDs), also referred to as crash test dummies. ATDs represent adult occupants in three body sizes: a large male, a midsize male, and a small female but do not represent the effect of soft tissues. With the advent of new advanced computers and the decreasing cost of computational resources, numerical simulations are currently used extensively to study road-traffic injuries. More details can be studied if occupants are modelled with numerical Human Body Models (HBMs). HBMs are numerical models based on human anatomy. Finite Element (FE)human body modelling, including anatomical structures represented in detail by elements, is a popular method for HBMs which is known as FEHBM. The

details of internal organs, bones, soft tissues and muscles are included in the FEHBMs, to provide a better understanding of the stresses and strains sustained by the human body [13, 14, 15, 16]. FEHBMs were initially developed to represent adult occupants in the same sizes as the ATDs. Hence, the sizes of current FEHBMs such as the Total Human Model for Safety (THUMS) [17, 18] and the Global Human Body Models Consortium (GHBMC) [19, 20] are similar the ATDs. As such, they are not fully representative of the obese population and thus, their use in studying obesity associated injuries, particularly submarining, is limited.

In addition to the shape and size of obese occupants, the material behaviour of adipose (fat) tissue may also influence the dynamics of responses and, subsequently the injury mechanism [21] during the interaction of the human body and the restraint system. For example, for lap belt to pelvis interaction, the material behaviour of adipose tissue may play an essential role in explaining how the lap belt fit observed in [6] influences the risk of submarining. However, to the best knowledge of the author, currently there is neither an appropriate constitutive model for adipose tissue in FEHBMs nor any investigations into how adipose tissue properties may influence the risk of submarining. The development and calibration of an adipose tissue constitutive model is challenging, firstly, due to only few reports being available on the mechanical testing of adipose tissue in the literature [22, 23, 24, 25, 26], and secondly, the intrinsic wide variations in the mechanical properties of adipose tissue at high strain rates and large deformations. For example, the non-monotonic dependence on strain rates exemplified in Fig. 1.1 indicate significant inter-sample variations and lacking repeatability in material testing.

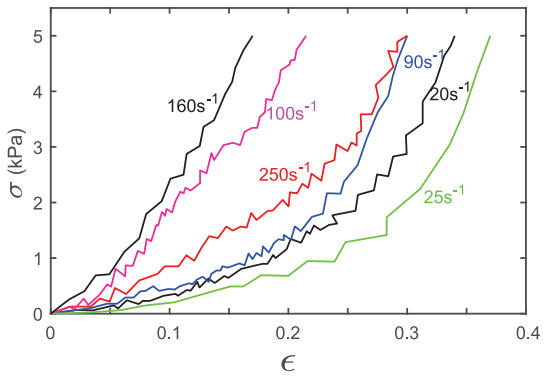

Figure 1.1: *Wide variations in mechanical properties of adipose tissue in an unconfined compression test in [22].*

1.2 Aim

The ultimate goal of this research is to advance the understanding of the role adipose tissue has in FEHBMs, focusing on the submarining mechanism and, in particular, how submarining is influenced by obesity and adipose tissue mechanical properties. This understanding is essential to design and improve safety measures as well as the biofidelity of FEHBMs.

This work addresses two levels: the tissue level and the human body level. The tissue level mainly deals with constitutive modelling of adipose tissue, while the human body level studies the submarining mechanism. The following key questions forms the centre of each study level.

- **Research questions at the tissue level:**
  - Which information can be obtained from different experimental setups used for characterising adipose tissue properties? (**Paper A**)
  - Considering the high variation in adipose tissue behaviour at large deformation and high strain rates, what is a reliable parameter identification for the adipose tissue constitutive model? (**Paper B**).
  - What is a suitable constitutive model to predict adipose tissue behaviour in vehicle crash situations? (**Paper A and B**).
- **Research questions at the human body level (submarining):**
  - What is the advantage of the new constitutive model for submarining prediction compared to the current material models in FEHBMs for adipose tissue? (**Paper C**).
  - What features of the adipose tissue influence the submarining behaviour the most? (**Paper C**).
  - What other parameters, including vehicle-design and occupant parameters influence the mechanism of submarining? How do obesity and initial lap belt position influence the outcome? (**Paper D**)

1.3 Method Outline

To address the research questions above, the study is carried out as follows: First, a constitutive model for adipose tissue was established based on literature findings. Then, an FE model for simulating common experimental setups of adipose tissue were constructed

in Matlab whereby material parameters were identified. To study the effect of adipose tissue behaviour on submarining, the constitute model was implemented in LS-DYNA (LSTC, Livermore, CA) and an FE pelvis model was built. Different parameters that may influence submarining were studied. Global Sensitivity Analysis (GSA) was used to identify which parameters influence the submarining mechanism the most.

2 The Tissue Level

This section details the concepts, motivation and methods used for addressing the research questions on tissue level.

2.1 Adipose Tissue Histology

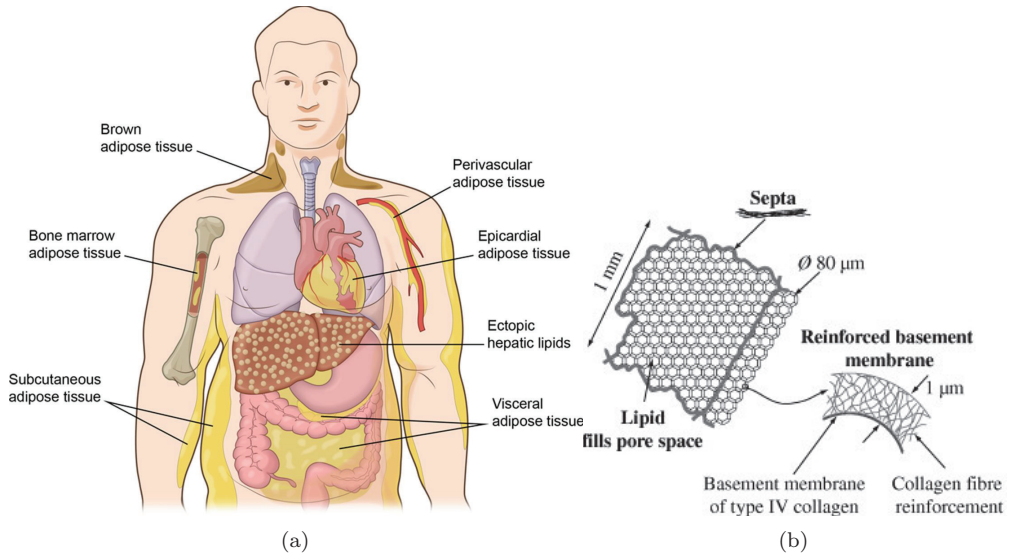

(a) (b)

Figure 2.1: *(a) Depot sites of adipose tissue and the anatomy, [27]. (b) Schematic of adipose tissue structure, [23].*

The adipose organ constitutes several depots located throughout the human body. These depots are mainly divided into visceral and subcutaneous adipose tissue. About 60–80% mass of adipose tissue is lipid, 5–30% mass is water and the remaining 2–3% mass is composed of proteins (collagen fibers). The tissue structure is a loose association of lipid-filled cells called white adipocytes, held in a framework of collagen fibers. Lipids within the white adipocytes are organised in one droplet. The diameter of the white adipocytes ranges from 30 to 70 μm, depending on the site of deposition. At a higher level, there is an open-cell foam-like structure called the interlobular septa, which contains adipocyte cells and is approximately 1 mm in size. The main stiffness of tissue comes from the collagen fibers surrounding the adipocyte cells. The volume fraction of the interlobular septa is sufficiently low to make its contribution to the macroscopic stiffness negligible [23]. Cross-link collagen fibers and their alignment provide nonlinear properties

to the tissue stiffness. A large amount of liquid in the tissue (mostly lipid droplets in cells) makes the tissue incompressible [23].

2.2 Adipose Tissue Mechanics

In a car crash, the impact between the human body and interior objects or interaction of the human body with the restraint system (e.g., seatbelt and airbag), are influenced by the mechanical behaviour of adipose tissue. The main motivation for considering adipose tissue predominantly single solid phase is the low level of extracellular fluid as well as the closed-cell structure of adipose tissue [23, 22, 25, 28, 26], opposed to more biphasic models of internal organs [29, 30, 31]. Adipose tissue is highly nonlinear at large deformation under impact loads in a car crash. Besides, the behaviour is rate-dependent, stiffening a few orders of magnitude during rapid loading [24, 22]. Therefore, the nonlinear and rate-dependent features must be incorporated into the constitute model of adipose tissue. Hyperelastic models are often used to reflect the nonlinear behaviour of soft tissue at quasistatic conditions. To characterise rate-dependent property either a complex modulus approach or a convolution integral approach is often used. A common test setup is rotational rheometer tests. By imposing a sinusoidal shear strain, $\gamma(t)$, on a sample a sinusoidal shear stress, $\tau(t)$, having a shift angle of δ to the excitation angle is obtained. The value of phase angle, δ, determines how viscoelastic a material is; $\delta = 0$ for a perfect elastic material and $\delta = \pi/2$ for a perfect fluid. So, frequency-dependent properties of shear stiffness and phase angle δ can be measured and expressed as:.

$$\begin{aligned} &\gamma(t) = \gamma_0 \sin(\omega t) \\ &\tau(t) = G_d(\omega)\gamma_0 \sin(\omega t + \delta) = G'\gamma_0 \sin(\omega t) + G''\gamma_0 \cos(\omega t) \\ &G_d = \sqrt{G'^2 + G''^2}, \quad \tan(\delta) = \frac{G''}{G'} \end{aligned} \tag{2.1}$$

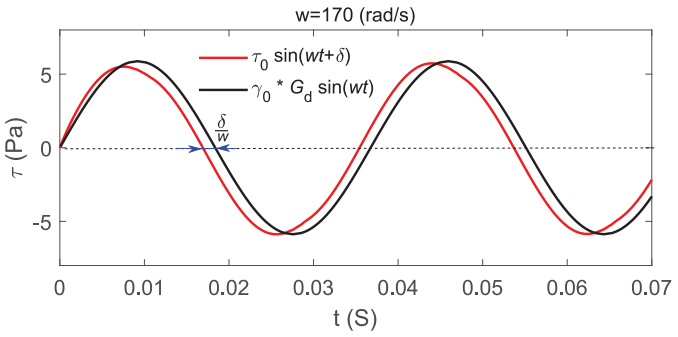

Figure 2.2: *A typical activation and response in rheometer tests,* $\gamma_0 = 0.001$.

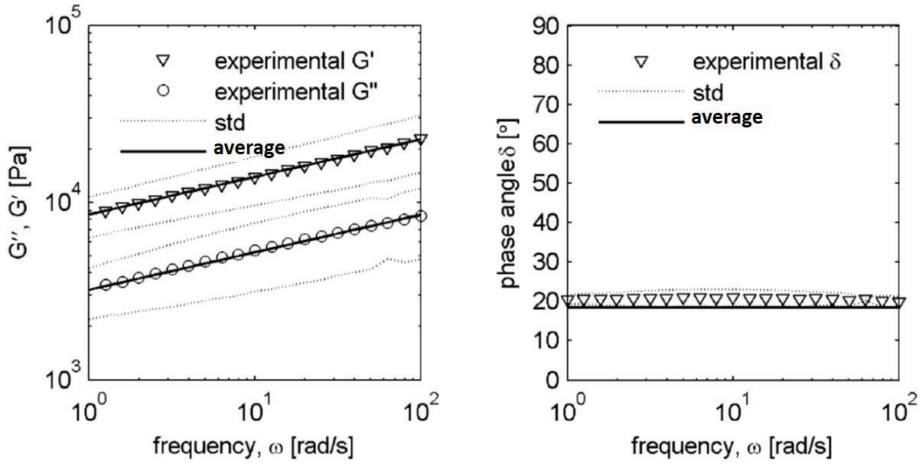

Figure 2.3: *Adipose tissue characteristics in the frequency sweep test in [24].*

where G' and G'' are the storage and loss modulus, respectively, and G_d is the frequency-dependent or dynamic shear stiffness. A convenient way to represent this response is by introducing a complex shear modulus.

$$G^\star = G' + iG'' \tag{2.2}$$

where $G^\star$ is the complex shear stiffness whose magnitude represents the dynamic shear modulus, $|G^\star| = G_d$. In frequency sweep tests, the behaviour of soft tissue can be characterised at a range of frequency, which gives a good overall picture of its rate-dependent behaviour. The frequency sweep test [24] on adipose tissue in the range of $1 - 100$ rad/s has showed that the rate-dependent shear stiffness of adipose tissue can be described by a power-law function, Fig. 2.3, as:

$$G'(\omega) = G'(1)\omega^p, \quad G''(\omega) = G''(1)\omega^p, \quad G_d(\omega) = G_d(1)\omega^p \tag{2.3}$$

where $G_d(1) = \sqrt{G'(1)^2 + G''(1)^2}$ is shear stiffness at the frequency ω =1 rad/ s and p is a material parameter related to the phase angle by $\tan(\delta) = \tan(p\pi/2)$, [32]. Regardless of the excitation frequency, a constant p value of 0.21, or a constant phase angle, has been measured for adipose tissue implying that the linear viscoelastic property is independent of strain rates, Fig. 2.3.

Convolution integral approach is motivated by relaxation experiments in which the time-dependent behaviour is attributed to time-dependent shear stiffness [33]. A widely used technique to describe the evolution of shear stiffness in time is the Prony series

approach [34, 35, 36, 26]:

$$G(t) = G_\infty + \sum_{k=1}^{n} G_k \exp(-t/\tau_k) \tag{2.4}$$

where G_∞ is the shear stiffness at equilibrium, τ_k are characteristic time constants, and G_k are associated shear stiffness weights with each time constant. The General Maxwell model for viscoelastic materials is a good illustration of this approach having one elastic chain for the equilibrium response in parallel with several viscoelastic chains to embed Prony series terms. Figure 2.4 compares the complex modulus approach with the Prony series in characterising rate-dependent behaviour. In the frequency sweep test, the continuous spectrum of the viscoelastic behaviour is described by a power-law function in Eq. 2.3. In the Prony series approach, it is discretely represented through incorporating a number of viscoelastic chains, Fig. 2.4. Each term in the Prony series approach is active, then, representing the rate-dependent behaviour at a certain frequency range. Moreover, there should be a constitutive relationship among Prony series terms to comply the continuous pow-law function of shear stiffness. In **Paper B**, this relation has been considered in the parameter identification of the adipose tissue material model.

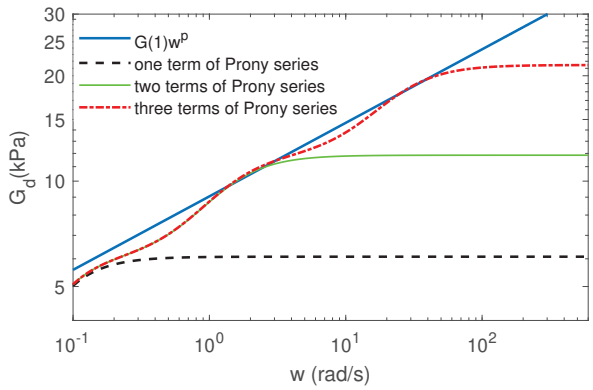

Figure 2.4: *Comparison of the complex modulus approach (the power-law function in [24]) and convolution integral approach (Prony series) in characterising shear stiffness at different loading rates.*

One limitation of the Prony series approach is that it is designed for linear viscoelastic behaviour which is less than 0.1% strain for adipose tissue [24]. Thus, this may impose a considerable limitation on the application of an adipose tissue model for road-traffic injuries as large deformation would be expected.

2.3 Constitutive Model

A constitute model is established to compute the material response at large deformations and high strain rates, features that are essential to model high-impact loading, It is here suggested to use the General Maxwell model, one block for equilibrium response in parallel with several viscoelastic blocks. A hyperelastic model is used as a baseline model for nonlinear elastic responses.

In the following section, the continuum formulation based on the multiplicative decomposition of the deformation gradient tensor is briefly introduced. Then, the strain energy function and derivation of elastic and viscoelastic stress terms have been presented.

2.3.1 Kinematics

The multiplicative decomposition approach enables the study of viscoelasticity in the setting of finite strains, i.e., large perturbations from the elastic equilibrium. The deformation gradient tensor $\mathbf{F}$ is multiplicatively decomposed into elastic, $\mathbf{F}_e$, and viscous parts, $\mathbf{F}_v$, as introduced in [37]. In computational biomechanics literature, the multiplicative decomposition framework was used to model brain tissue [38, 39]. The viscous part, $\mathbf{F}_v$, transfers the initial configuration to the intermediate configuration. Then, the $\mathbf{F}_e$ transfers the intermediate configuration to the current configuration. Therefore, large inelastic strains can be modelled. To model adipose tissue at a wide range of loading rates, the General Maxwell model is used as the finite viscoelastic model. It incorporates one elastic chain for equilibrium response (EQ) in parallel to N chains of Maxwell type for the non-equilibrium response (NEQ). Adding more NEQ chains covers a wider range of impact rates for adipose tissue.

$$\begin{aligned} &\mathbf{F} = \mathbf{F}_e^{(k)}\mathbf{F}_v^{(k)}, \quad k = 1, 2, ..., N \\ &\mathbf{C}_e^{(k)} = [\mathbf{F}_e^{(k)}]^T\mathbf{F}_e^{(k)} = [\mathbf{F}_v^{(k)}]^{-T}\mathbf{C}[\mathbf{F}_v^{(k)}]^{-1} \end{aligned} \tag{2.5}$$

Accordingly the rate of deformation $\mathbf{L}$ is also decomposed into two tensors:

$$\begin{aligned} &\mathbf{L} = \mathbf{L}_e^{(k)} + \mathbf{L}_v^{(k)}, \quad \mathbf{L}_e^{(k)} = \dot{\mathbf{F}}_e^{(k)}[\mathbf{F}_e^{(k)}]^{-1} \\ &\mathbf{L}_v^{(k)} = \mathbf{F}_e^{(k)}\dot{\mathbf{F}}_v^{(k)}[\mathbf{F}_v^{(k)}]^{-1}[\mathbf{F}_e^{(k)}]^{-1} \end{aligned} \tag{2.6}$$

2.3.2 Kinetics

The right Cauchy-Green deformation tensor $\mathbf{C}_e$ in intermediate configurations, Eq. 2.5, and the deformation gradient tensor $\mathbf{F}$ are used to express the total strain energy per

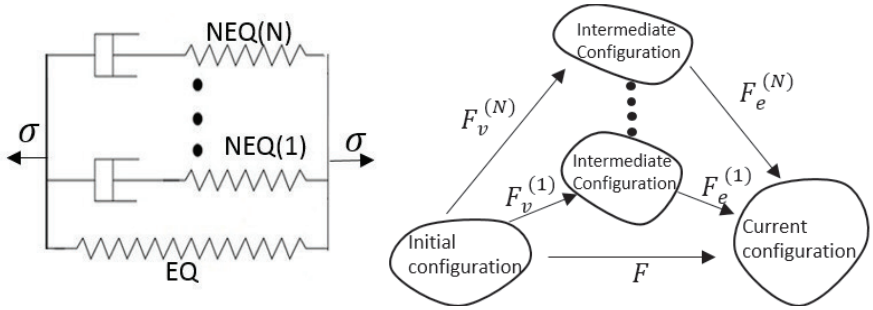

(a) (b)

Figure 2.5: *(a) General Maxwell model (b) Schematic representation of the multiplicative decomposition of the deformation gradient tensor* $\boldsymbol{F}$*, [37].* $\boldsymbol{F}_v$ *is the inelastic part of* $\boldsymbol{F}$*, which transfers the initial configuration to the intermediate configuration. Then* $\boldsymbol{F}_e$*, the elastic part of* $\boldsymbol{F}$*, transfers the intermediate configuration to the current configuration.*

unit volume as:

$$\Psi(\mathbf{F}, \mathbf{F}_v^{(1)}, \mathbf{F}_v^{(2)} ..., \mathbf{F}_v^{(N)}) = \Psi^{EQ}(\mathbf{F}) + \overbrace{\sum_{k=1}^{N} \Psi^{NEQ(k)}(\mathbf{C}_e^{(k)})}^{=\Psi^{NEQ}} \tag{2.7}$$

Adipose tissue has usually been assumed in literature to be incompressible material [23], however since adipose tissue response under impacts is studied herein, it has been considered as a nearly incompressible material. Therefore, to keep better control of the extent of incompressibility, the strain energy function Ψ in Eq. (2.7) has been split further into volumetric U and deviatoric parts $\hat{\Psi}$. A polynomial function is considered for the deviatoric part.

$$\begin{aligned}
&\Psi = \overbrace{\hat{\Psi}^{EQ}(\mathbf{F}) + U^{EQ}(J)}^{=\Psi^{EQ}} + \overbrace{\sum_{k=1}^{N} \left(\hat{\Psi}^{NEQ(k)}(\mathbf{C}_e^{(k)}) + U^{NEQ(k)}(J^{(k)}) \right)}^{=\Psi^{NEQ}} \\
&\hat{\Psi}^{NEQ(k)} = A_1^{(k)}(\hat{\mathrm{I}}_{\mathbf{C}_e}^{(k)} - 3) + A_2^{(k)}(\hat{\mathrm{I}}_{\mathbf{C}_e}^{(k)} - 3)^2, \quad \hat{\Psi}^{EQ} = A_1^{(e)}(\mathrm{I}_{\mathbf{C}} - 3) + A_2^{(e)}(\mathrm{I}_{\mathbf{C}} - 3)^2 \\
&U^{NEQ(k)} = \frac{\kappa_v^{(k)}}{2}(J^{(k)} - 1)^2, \quad U^{EQ} = \frac{\kappa_e}{2}(J - 1)^2
\end{aligned} \tag{2.8}$$

where $J = \det(\mathbf{F})$ and $J^{(k)} = \det(\mathbf{F}_e^{(k)})$ are the Jacobians of related deformation gradient tensors, A_1 and A_2 are material parameters and κ is also a material parameter which

physically means bulk stiffness for each chain. This enables the effective bulk stiffness being related to strain rate, avoiding too soft bulk stiffness at high loading rates. Moreover, $\mathrm{I}_{\mathbf{C}}$ =tr($\mathbf{C}$) and $\hat{\mathrm{I}}_{\mathbf{C}_e}$ are the first invariants of $\mathbf{C}$ and $\hat{\mathbf{C}}_e$. Correspondingly, the second Piola-Kirchhoff stress consists of elastic and inelastic contributions which are calculated from equilibrium and non-equilibrium parts, respectively.

$$\mathbf{S} = 2\frac{\partial \Psi^{EQ}}{\partial \mathbf{C}} + 2\sum_{k=1}^{N}[\mathbf{F}_v^{(k)}]^{-1}\left(\frac{\partial \Psi^{NEQ(k)}}{\partial \mathbf{C}_e^{(k)}}\right)[\mathbf{F}_v^{(k)}]^{-T} = \mathbf{S}^{EQ} + \mathbf{S}^{NEQ} \tag{2.9}$$

The term $\mathbf{S}^{NEQ}$ corresponds to the viscous stress which accounts for the energy absorption of adipose tissue. According to adipose tissue behaviour in a wide range of strain rates [25, 22], it has highly rate-dependent property where it stiffens up exponentially to a few orders of magnitude at high strain rates. On the other side, as the viscous stress ($\mathbf{S}^{NEQ}$) evolves within the tissue (e.g., at higher strain rates or large deformation), it relaxes quicker, a property which is referred to as softening behaviour [25]. To account for this property, a nonlinear viscous relation is considered for the evolution of the viscous stress ($\mathbf{S}^{NEQ}$). As suggested in [37], the evolution rule for each viscous chain is given as:

$$\dot{\mathbf{F}}_v[\mathbf{F}_v]^{-1} = \Lambda\frac{3\bar{\mathbf{M}}_{dev}}{2\tau_{eq}^{NEQ}}, \quad \Lambda = \frac{1}{t_\star}\eta(\tau_{eq}^{NEQ}) \tag{2.10}$$

where $\mathbf{M}_{dev}$ is the deviatoric part of Mandel stress and τ_{eq}^{NEQ} is the von Mises stress of the overstress. To incorporate the softening behaviour of adipose tissue [24, 25], the overstress function η has been defined as a power-law function of τ_{eq}^{NEQ} in which n_c is the exponent ($n_c > 1$ for nonlinear viscoelasticity) and τ_c is scalar corresponding to the stress in linear viscoelastic regions.

$$\eta(\tau_{eq}^{NEQ(k)}) = \left(\frac{\tau_{eq}^{NEQ(k)}}{\tau_c}\right)^{n_c} \tag{2.11}$$

2.4 FE Modelling of Adipose Tissue Test Setups

Adipose tissue samples are usually tested in one of the following experimental setups: confined and unconfined compression tests, indentation tests, or rotational rheometer tests. In Fig. 2.6 these setups, including possible loading conditions, are shown. For example, the rotational rheometer test, may involve a simple ramp loading-unloading or a sinusoidal excitation in which a sinusoidal shear strain, $\gamma(t) = \gamma_0 \sin(wt)$, is imposed at a certain frequency, in the steady state, a sinusoidal shear stress, $\tau(t) = \tau_0 \sin(wt + \delta$ with a shift angle of δ is measured. In order to study these test setups and for model calibration in **Paper A** and **Paper B**, a finite element model of the setups is developed.

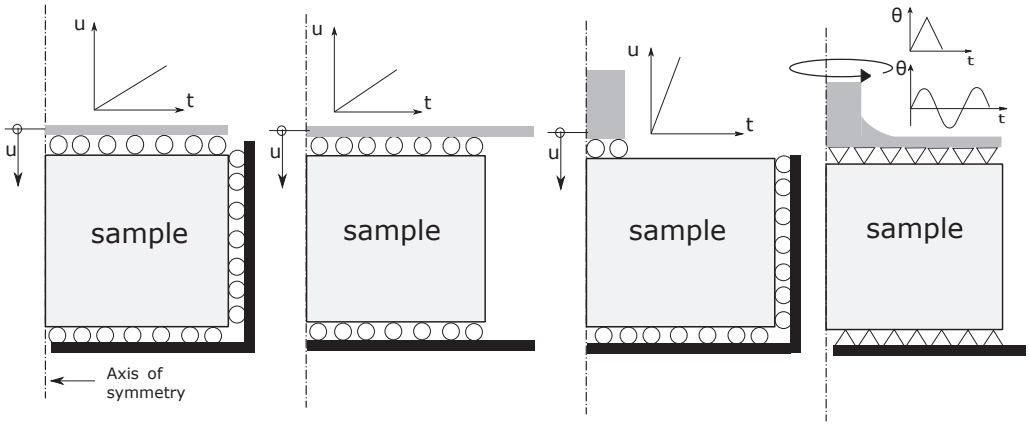

Figure 2.6: *Illustration of experimental setups including loading and boundary conditions. From left to right: confined and unconfined compression tests, indentation tests, and rheometer tests; Circles: frictionless contact; Triangles: fully clamped boundaries; Black: stationary parts; and Grey: moving parts.*

Due to the symmetry of loads, boundary conditions and samples geometry for all of the setups, constant displacement field with respect to Θ direction is expected in samples, i.e., $\frac{\partial(\bullet)}{\partial(\Theta)} = 0$. This also applies to the rheometer setup with $v \neq 0$. Therefore, stress is also symmetric Fig. 2.7. Thus, the 3-D experimental setups can be represented by considering the $RZ-$plane and a 2-D finite element model should suffice, Fig. 2.8. However, there are still 3 displacement-degrees of freedom for each node. The finite element model of these experimental setups is presented in cylindrical coordinates (as the cylindrical shape of samples). The undeformed position vector, $\mathbf{X}$, the deformation vector, $\mathbf{u}$, and the deformed position vector, $\mathbf{x}$, are defined using unit vectors $\mathbf{e}_R$, $\mathbf{e}_\Theta$ and $\mathbf{e}_Z$ in the radial, circumferential and axial directions, respectively.

$$\begin{aligned} &\mathbf{X} = R\mathbf{e}_R + Z\mathbf{e}_Z, \quad \mathbf{u} = u\mathbf{e}_R + v\mathbf{e}_\Theta + w\mathbf{e}_Z \\ &\mathbf{x} = \mathbf{X} + \mathbf{u} \end{aligned} \tag{2.12}$$

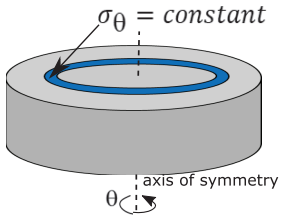

Figure 2.7: *Stress is symmetric for all of the test setups presented in Fig. 2.6.*

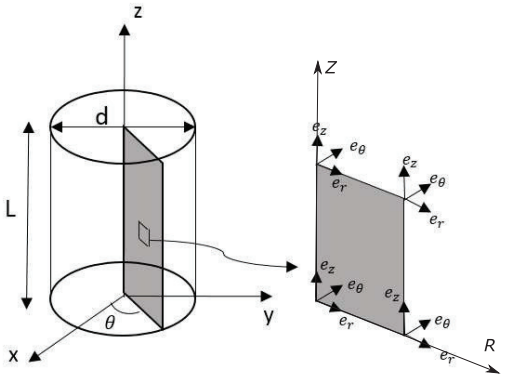

Figure 2.8: *The finite element model for adipose tissue samples and its four node quadrilateral element in cylindrical coordinates.*

where R and Z are the undeformed radial and axial coordinates, and u, v and w are the displacements in the direction of cylindrical coordinate unit vectors, R, θ and Z, respectively. The following discretisation has been applied to the displacement field:

$$u = \sum_{i=1}^{4} N_i(r,z)u^{(i)}, \quad v = \sum_{i=1}^{4} N_i(r,z)v^{(i)}, \quad w = \sum_{i=1}^{4} N_i(r,z)w^{(i)} \tag{2.13}$$

The corresponding deformation gradient tensor $\mathbf{F}$ becomes:

$$\mathbf{F} = \begin{bmatrix} 1+\frac{\partial u}{\partial R} & -\frac{v}{R} & \frac{\partial u}{\partial Z} \\ \frac{\partial v}{\partial R} & 1+\frac{u}{R} & \frac{\partial v}{\partial Z} \\ \frac{\partial w}{\partial R} & 0 & 1+\frac{\partial w}{\partial Z} \end{bmatrix} \tag{2.14}$$

Introducing the total Lagrangian formulation [40], the momentum balance equation takes the following form after applying the spatial discretisation:

$$M\ddot{U} + F_{int}(\dot{U}, U, t) = F_{ext}(t) \tag{2.15}$$

where M is the mass matrix, F_{int} is the nodal forces equivalent to the element stress and F_{ext} is the nodal loads corresponding to externally applied displacements. The transient analysis of this nonlinear problem is carried out using direct time integration of the equation of motion. For reliable solutions, a stable and efficient time integration algorithm is desirable. Methods that are unconditionally stable in linear analyses appear to be a natural choice for use in nonlinear analyses. However, unfortunately they might not remain stable for nonlinear analyses in large deformation as the traditional methods, such

as the trapezoidal rule and the Wilson θ-method, did not give a stable solution for the Eq. 2.15. Instead, a composite implicit time integration procedure [41] was used, which is more effective for producing stable solutions for nonlinear dynamic problems [41, 42]. The time step Δt has been subdivided into two equal sub-steps. For the first sub-step, the trapezoidal rule was used and for the second sub-step, the 3-point Euler backward method was employed. The equation of motion Eq. 2.15, after time integration, was coded and solved in Matlab R2015b.

2.5 Verification

Verification and validation are processes by which evidence is generated and credibility is thereby established that a computer model yields results with sufficient accuracy for its intended use [43]. More specifically, verification is the process of determining that a model implementation accurately represents the conceptual description and solution of the model [44]. In simple terms, verification deals with *solving the equations right* whereas validation is the process of *solving the right equations*. The verification process is generally divided between code verification and calculation verification [45, 43, 46]. Code verification assesses whether the code is an accurate representation of the discretised model, whereas calculation verification determines whether the discretised model correctly represents the mathematical model. A thorough verification process, specially code verification, is necessary when "custom" or "in-house" computational codes are developed. The benchmark hierarchy that is usually recommended for model verification is: 1- analytical solutions; 2- semi-analytical solutions; 3- numerical solutions. However, since the implementation of a nonlinear viscoelastic model in the finite strain computational framework is to be verified, no analytical or semi-analytical solution is available. The numerical solution to the intended problem is also limited because, to the best of the author's knowledge, the current nonlinear viscoelastic constitutive model could not be found in any commercial software. Therefore, in the earlier part of the study, the model was only justified by being compared to the known physical features of rheometer tests. However, in the second part of the work associated with the Human Body Level, when the material model of adipose tissue was implemented in LS-DYNA as a user-defined material model, further verification was carried out. Similar results were obtained from the model in Matlab and numerical solution in LS-DYNA, consequently allowing verification of the model in Matlab and the accurate implementation of the constitutive model of adipose tissue in LS-DYNA.

There are some physical features in rotational rheometer tests that are suitable for justifying the computational model of adipose tissue including the constitutive model,

the element type and the composite implicit time integration scheme. As mentioned in Eq. 2.1, in a rotational rheometer test, the sinusoidal shear strain of $\gamma(t) = \gamma_0 \sin(wt)$ is imposed at a specific frequency which in the steady-state results in sinusoidal shear stress, $\tau(t) = \tau_0 \sin(wt + \delta)$. The phase angle δ and the dynamic shear stiffness G_d are the two characteristics of this test which were well captured by the adipose tissue model in Fig. 2.2. Different frequencies with different viscoelastic parameters were simulated, resulting in the same qualitative response [47]. It is mentionable that traditional methods such as the trapezoidal rule and the Wilson θ - method did not give a stable solution. Also, full integration formulation was employed since under-integrated formulation did not converge.

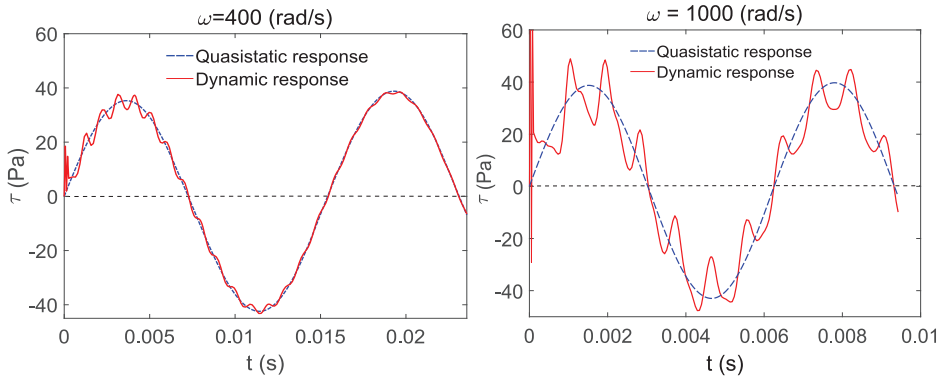

Figure 2.9: *The difference between the dynamic and quasi-static behaviour of adipose tissue at two frequencies,* $\gamma_0 = 0.001$.

The tissue response from rotational rheometer tests is usually analysed with the Fourier transform and only the first mode corresponding to the equilibrium response, known as constitutive tissue behaviour, is taken as the tissue response to rheometer tests. So, to characterise the tissue response at very high rates, the application of the rotational rheometer setup is limited since the inertia effect becomes dominant, and the separation of equilibrium response from the dynamic response might not be transparent anymore. To investigate this assumption as well as the capability of our model to capture this physics, quasi-static and dynamic responses of a typical rheometer test were modelled at two high frequencies of $w = 400$ rad/s and $w = 1000$ rad/s. The apparent stress $\tau = \frac{2T}{\pi R^3}$ is calculated form the reaction torque at the upper plate, T. At the frequency of $w = 400$ rad/s, Fig. 2.9, a slight inertia effect was seen at the beginning of the adipose tissue response, which quickly damps out because of the viscoelastic property of adipose tissue (hysteresis energy dissipation). Hence, in this case, the equilibrium response of the adipose tissue equals its steady response. However, raising the frequency to $w = 1000$

rad/s, the inertia effect becomes more dominant which can limit the extraction of the equilibrium response (or the constitutive behaviour).

Another limitation of rheometer tests is the sample size. A high length-to-diameter of a sample may also activate the inertia effect [48, 24]. The sample size proportion L/d is doubled in Fig. 2.8 and the consequent effect has been investigated. The increase of L/d for the sample activates the inertia effect as it is now more dominant, Fig. 2.10. Therefore, the quasi-static assumption might not be reasonable for this sample size, whereas, for half of this sample length, it is a reasonable assumption. Any limitations to the frequency level and the sample size of the rheometer tests for adipose tissue has been appropriately addressed by the developed model. Moreover, the model captured the known tissue behaviour in rheometer tests at high frequencies. These observations enhance our confidence in the model.

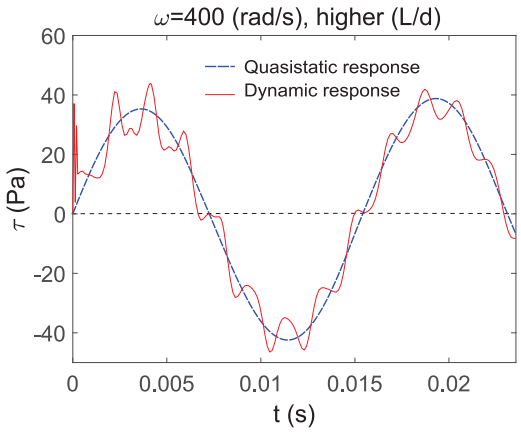

Figure 2.10: *The effect of a larger length-to-diameter* (L/d) *size on adipose tissue behaviour,* $\gamma_0 = 0.001$.

3 The Human Body Level

This section introduces the methods applied for studying submarining, considering variability in occupant anthropometry and material properties, as well as variability in vehicle design parameters. To the best of the author's knowledge, a ubiquitous quantitative definition of submarining has not been defined to date. However, the consensus is that the qualitative definition of submarining pertains to the lap belt suddenly slipping over the Anterior Superior Iliac Spine (ASIS) [49, 21, 8]. Initially, the proposed adipose tissue constitutive model was implemented in LS-DYNA. Some initial efforts were made to study the submarining behaviour using a full FEHBM, the SAFER HBM v9 [50, 51]. However, the soft behaviour of the new constitute model for adipose tissue in combination with poor mesh quality in the pelvic region resulted in numerical issues, which motivates the continuing study using a FE submodel of the pelvis [21] that can easily be remeshed. The FE submodel's potential to sufficiently show submarining characteristics has been verified. Finally, the submarining phenomenon and the influence by different levels of obesity and lap belt initial position, have been studied.

3.1 Implementation in FEHBM

The new constitute model of adipose tissue was implemented in LS-DYNA. This required converting the Matlab code into a Fortran subroutine, which takes the deformation gradient tensor as input and returns the Cauchy stress tensor as output. The Fortran subroutine output for a given deformation gradient tensor was compared with the Matlab code to ensure that conversion from Matlab code to Fortran code had been accurately performed. In addition, the rotational shear tests were recreated in LS-DYNA and compared with the results of the computational model in Matlab. Subsequently, the correct implementation of the new material model in LS-DYNA, as well as the computational model itself, were verified. This was repeated for different strain levels and strain rates obtaining the same results as the computational model in Matlab. Both under-integrated and fully integrated element formulations produced stable results, probably because high-quality fine hexahedral elements were used. In the next phase, the full SAFER HBM v9 [50, 51] model was used to replicate the PMHS test PMHS700 in [49]. Although this time, several numerical instability issues were encountered.

The numerical instability was mainly due to poor mesh quality. The aspect ratio for some of the elements for adipose tissue in the SAFER HBM v9 are high. Under lap belt loading, adipose tissue deformed sharply which resulted in skewed elements, and consequently numerical error. This does not present a problem with the default material

model for adipose tissue as it is much stiffer, preventing significant deformation and consequently generating less of numerical instability. One particular issue with explicit FE codes such as LS-DYNA when using an under-integrated scheme involves hourglass modes. Hourglass modes are nonphysical, zero-energy modes of deformation that produce zero strain and no stress. LS-DYNA has various algorithms for preventing hourglass modes which normally introduce an artificial numerical stiffness into the model. It is recommended (by LS-DYNA Support) that hourglass energy should be $< 10\%$ of the peak internal energy of each part and that hourglass control of viscous type is used for soft materials. However, when using the viscous type hourglass control, the hourglass energy of adipose tissue in SAFER HBM v9 was more than 50% of the internal energy. Full integration formulation caused numerical instability at the very early simulation time, possibly due to volumetric locking. Last but not least, numerical instability was observed when (a soft material model such as) the adipose tissue model was integrated in between other stiff parts in the SAFER HBM v9. In this case, the sharp shift in the material behaviour at boundaries between stiff and soft parts caused numerical problems.

Certain practical concerns associated with submarining study prevail, particularly if the effect of different obesity levels and initial lap belt position on submarining are to be studied. Such cases require building different geometries with different subcutaneous adipose tissue layer thicknesses, which are very difficult and time consuming to build in a full FEHBM. In addition, following specifics of a test setup such as the initial belt position can be challenging in a full FEHBM, since the belt position has to be adapted to the contour of the body surface.

Due to the mentioned numerical and practical issues, constructing an FE submodel of the pelvis and its surrounding tissue able to capture the main characteristics of the submarining phenomenon, while still remaining simple enough to be meshed with high-quality elements, was chosen over established full FEHBMs.

3.2 The FE Pelvis Submodel

Since the interaction between the lap belt and the pelvis is a local phenomenon, only involving parts surrounding the pelvis influencing submarining, have been the focus of this study. Therefore, inspired from the SAFER HBM v9 [50, 51], the developed model only features the flesh (skin and subcutaneous adipose tissue), the abdomen and part of the pelvis (iliac crest), Fig. 3.1. Submarining , in this study, has been investigated in a simplified setup, pulling the lap belt over a fixed pelvis similar to in [49, 52, 8, 53]. The posterior side of the abdomen has been fixed to resemble the strong force from the fixed spinal column. The flesh tissue is very soft and deforms sharply under the lap belt

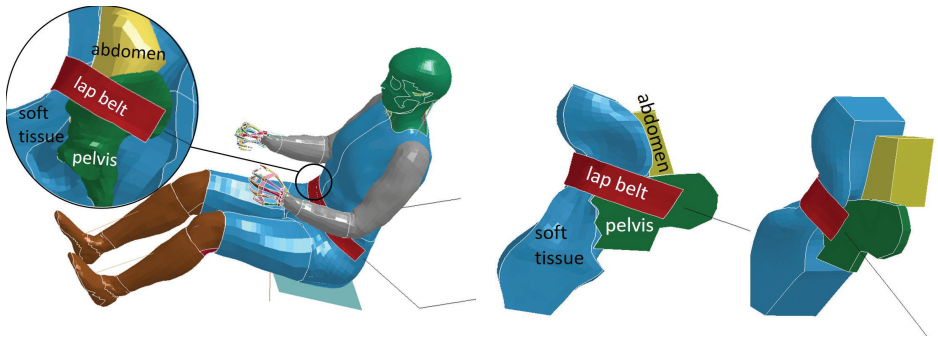

(a) (b)

Figure 3.1: *(a) SAFER HBM v9 model and the details of the area of interest to study lap belt-pelvis interaction. (b) Modelling the area of interest by a FE pelvis submodel (two different perspectives).*

load, so the effect of the imposed deformation on tissue response is negligible at a short distance from the lap belt. This has been confirmed through different simulations where the type of boundary condition of the soft tissue was altered without influencing the model response. Due to the symmetry in the lap pulling test setup, only one side of the lap belt-pelvis interaction has been modelled.

The formulation of the conceptual model is the most important aspect of the modelling process. The physical responses of interest must be captured in the computer model, hence it is essential to initially determine the intended use of the model and to identify a-priori which components to implement and which to leave out. At this point, it should be assured that the conceptual model is based on a rational assumption, i.e., in this case the only parts engaged during lap belt loading are soft tissue, pelvis, and abdomen. These parts have been investigated through a full FEHBM model analysis. A virtual belt pulling test using a morphed SAFER HBM v9 representative of a female with a BMI of 31 corresponding to the PMHS in [49] was simulated in LS-DYNA. The default material model for adipose tissue was replaced with the new material model in this simulation. The lap belt force and the contact force between the soft tissue and the pelvis as a function of time are presented in Fig. 3.2. The corresponding belt trajectory is also shown. To synchronise the two figures, the three specific moments of a, b and c are marked on both curves. Three phases are recognisable in Fig. 3.2. In the beginning, the lap belt force was solely resisted by the pelvis through the soft tissue until it reached its peak, i.e., the lap belt force was almost the same level as the pelvis-soft tissue contact force, (Phase I, from a to b). In this phase, secure hooking between the lap belt and the pelvis was formed. Then, due to accumulated force between the pelvis and the lap belt, a drop in the belt

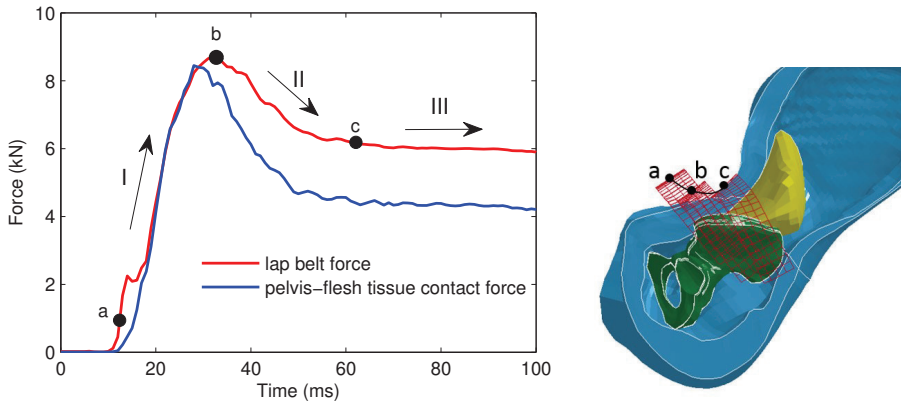

(a) (b)

Figure 3.2: *(a)The lap belt force and pelvis-soft tissue contact force over time for the morphed SAFER HBM v9. (b) The corresponding belt trajectory. Three specific moments of a, b, and c are marked on both curves.*

force occurred as the result of the belt slipping over the iliac crest. At this moment, the abdomen started to engage and take some of the lap belt force which is recognisable in Fig. 3.2. The belt force differs from the pelvis-soft tissue contact force (Phase II, from b to c). Finally the lap belt slipped off completely and loaded the abdomen which created a constant low force (Phase III, after c). Therefore, all deformation occurred locally around the iliac crest and can be sufficiently described by only considering the complex of the lap belt-soft tissue-pelvis-abdomen. A similar qualitative response of belt force was also observed in the lap belt pulling tests conducted by [49], thus, supporting the assumption of the conceptual model herein.

3.3 Verification and Validation

The solution to submarining simulation with the FE pelvis submodel is smooth, i.e., there are no singularities, discontinuities and unrealistic buckling in the behaviour. Therefore, the calculation verification in this case is simply assumed as incrementally refining element discretisation until a convergent result is obtained. It is always recommended that the intended validation parameter (e.g., strain measurements) be used as the primary criteria for determining mesh convergence [54]. However, since submarining does not have a quantitative definition and involves interaction among many physical parameters resulting in a particular behaviour, there is no quantifiable validation parameter for determining mesh convergence. Hence, the lap belt force might be the best choice criteria for the mesh

convergence. An average element size of 10 mm provided convergent results, meaning that smaller element sizes did not meaningfully influence the belt force. Hexahedral elements incorporating full-integrated formulation, (LS-DYNA element formulation 2) were used for the solid parts of the FE pelvis submodel. The skin, lap belt, and the cortical bone of the pelvis were meshed with shell elements. Since high-quality elements were generated for the adipose tissue, the FE pelvis submodel did not encounter any of the instability issue which was previously observed in the full SAFER HBM v9.

In the next step, the FE pelvis submodel will be validated. A comprehensive validation for the FE pelvis submodel might not be achievable since there is no well-quantified measure for submarining. Instead it is a sequence of physical processes leading to a binary outcome, submarining or not submarining. However, comparing the qualitative response of the model with a few physical tests may still provide more evidence of the reliability of the FE pelvis submodel. For this purpose, the lap belt pulling tests conducted by Kim et al. [49] were simulated. Four tests on an obese PMHS (BMI = 31), defined as PMHS700 in the paper [49] which resulted in submarining, together with one test on a non-obese PMHS (BMI = 24.1), PMHS683, without submarining were selected. The initial belt position was given with respect to the ASIS, as in the test [49]. Pelvis angle and initial belt angle were also modelled as reported in the test [49]. Two different loading rates of 3 m/s and 4 m/s and two load limit levels of 1 kN and 3 kN were used. The thicknesses of the soft tissue around the ASIS of the obese PMHS700 and the non-obese PMHS683 were different, 40 mm and 15 mm, respectively, which were also considered in the FE pelvis submodel. Lap belt force and belt trajectory of each lap belt pulling test are shown in Fig. 3.3. Similar to the physical test, the FE pelvis submodel predicted submarining for all load cases in the PMHS700 and not submarining for the load case in the PMHS683. In contrast to the newly developed material model [55], the default material models in the GHBMC (a foam model defined by a single uniaxial load curve) and the THUMS v3 (a linear elastic model with one term of Prony series) did not result in submarining for any load case in the PMHS700. Hence, simulation of the physical tests in [49] at least provided some support to the FE pelvis submodel as well as the biofidelity of the new material model for submarining prediction.

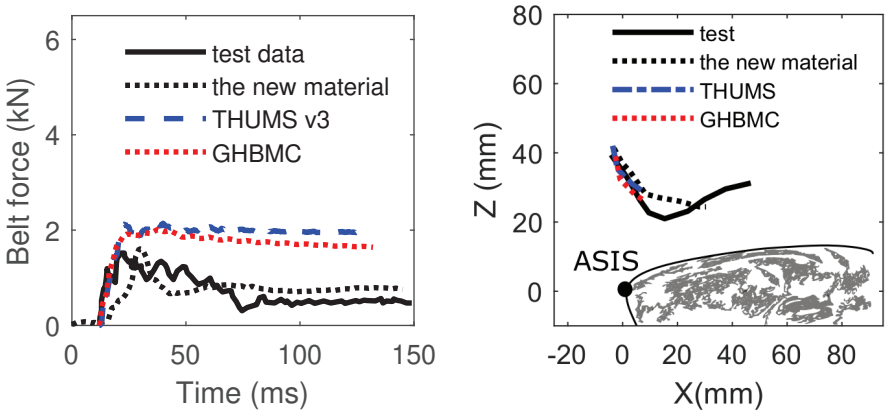

(a) *PMHS700-3*

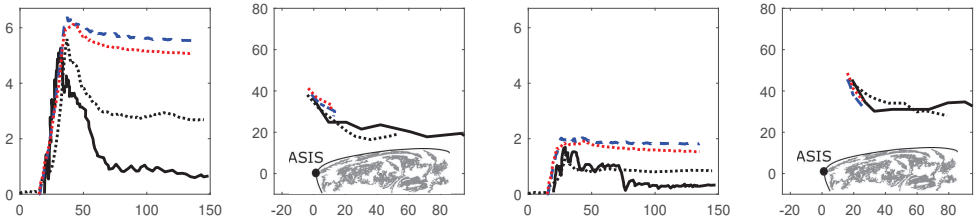

(b) *PMHS700-4*

(c) *PMHS700-5*

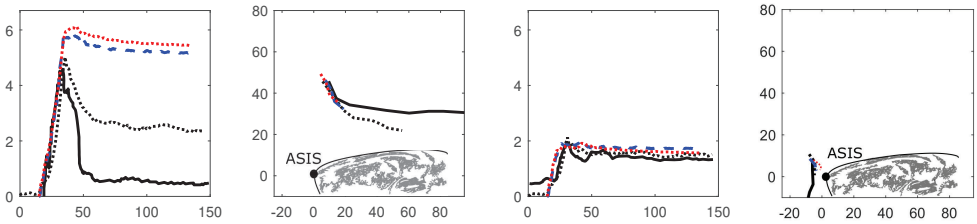

(d) *PMHS700-6*

(e) *PMHS683-3*

Figure 3.3: *The model prediction of the lap belt pulling test [49] on two PMHSs, the PMHS683 and PMHS700, comparing new material model [55], the THUMS v3 and the GHBMC material models. The first figure for each set is the lap belt force and the second one is its corresponding belt trajectory.*

3.4 Submarining Simulation

This section explains how submarining, and in particular the effect of initial lap belt position and the thickness of adipose tissue, can be evaluated by the FE pelvis submodel. The qualitative definition of submarining pertains to the lap belt suddenly slipping over the ASIS [49, 21, 8]. However, to carry out a parameter study, submarining should be determined in the simulation by a measurable quantity. In the current study and assigning the ASIS as the origin of coordinates for the midpoint belt position, submarining has been quantified as the trajectory of the midpoint of the lap belt passing beyond $X > 25$ mm, Fig. 3.5. The reason for selecting 25 mm is because it is half of the width of a typical belt, i.e., the midpoint, and passing the midpoint of the lap belt from $X = 25$ mm means the whole belt will have slipped over the ASIS. Hence, submarining would probably be unavoidable. The accuracy of determining submarining with this criterion is also visually confirmed. As an example, Fig. 3.4 shows a typical submarining simulation result, where cases identified as submarining are defined in red, whereby accurate submarining identification can be checked.

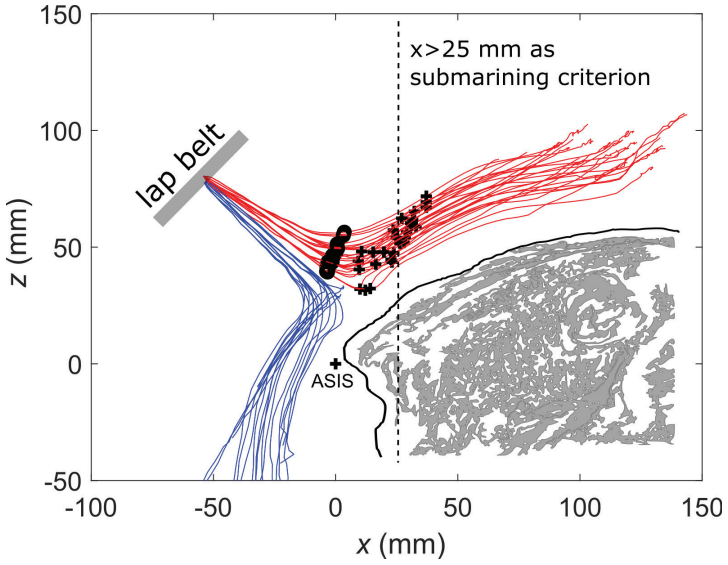

Figure 3.4: *All belt trajectories starting from one point; the cases identified as submarining are defined in red [21].*

As mentioned, obesity influences the lap belt initial position due to a thick layer of adipose tissue [6, 5]. An increase in BMI moves the lap belt initial position further anterior-superior to ASIS, approximately in a 45° direction [6]. Correspondingly, this has

been accounted for in the FE pelvis submodel through consideration of four different soft tissue thicknesses, Fig. 3.5. Comparing the lap-belt position and BMI in [6, 4], the FE pelvis submodel will approximately cover the BMI range of $25 - 40$, with five BMI steps between each layer. Moving the lap belt position along these curves, the space in the front of the ASIS can be swept by defining 10 points along each curve, Fig. 3.5. This computational setup facilitates investigation of various parameters that may influence submarining.

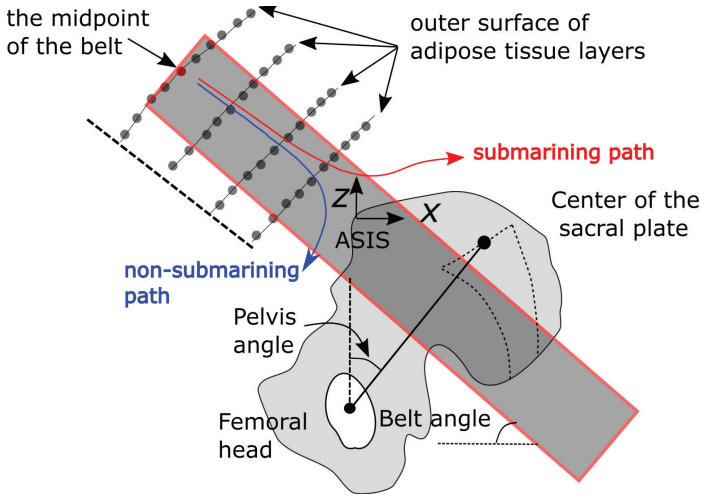

Figure 3.5: *The four curves represent the outer surface of soft tissue with different thicknesses of adipose layers. The dots represent the possible initial lap belt positions (the midpoint of the belt). The pelvic angle, as defined in [56], is the line through the midpoint of the sacral plate and midpoint of the femoral head's axis, and the vertical. The belt angle is the angle between the lap belt and the horizontal in the sagittal (XZ) plane.*

4 Global Sensitivity Analysis

A wide individual spread of mechanical properties is an intrinsic characteristic of biological materials including adipose tissue, particularly at high-impact loading. Therefore, it is common that as an initial procedure for understanding the physical response of a system in the field of biomechanics sensitivity analysis is performed. Global Sensitivity Analysis (GSA), [57], has been commonly used for this purpose in computational biomechanics literature [54, 58, 59, 60, 61]. The GSA can be used in different circumstances for different purposes and the manner of their use in one content might be inappropriate for another, [62]. Hence, the formulation of GSA inquiry, also called *setting*, should be stated before carrying out GSA. The *factor prioritization* (FP) setting is associated with obtaining insight into the most important input parameters of a particular system, which has been used in this study [58, 21]. When input parameters do not correlate, Sobol [63] has suggested a variance-based GSA in the FP setting. The method is based on the decomposition of the total output variance. If an output variable Y depends on a vector of n independent random variables, $\mathbf{X} = [X_1, X_2, ..., X_n]^T$, via a function as $Y = h(\mathbf{X})$, then the total variance V_Y can be decomposed as:

$$V_Y = \sum_{i=1}^{n} V_i + \sum_{i<j} V_{ij} + \sum_{i<j<k} V_{ijk} + ... \tag{4.1}$$

where V_i is the expected reduction in V_Y as a result of fixing X_i. It is also referred to as primary variance. Similarly, V_{ij} considers the effect of interaction between X_i and X_j on V_Y. Then, the primary sensitivity S_i is expressed as $\frac{V_i}{V_Y}$, [64] . Likewise, the sensitivity indices of all higher-order variance components, e.g. $S_{ij} = \frac{V_{ij}}{V_Y}$, can be obtained. Global sensitivity S_{Ti} focuses on the reduction in total variance V_Y when the primary variance, V_i, and all higher-order variance components having i in their subscript are neglected, [65].

In general, computing sensitivity coefficient by ANalysis Of VAriance (ANOVA) decomposition involves two-layer high-dimensional integrals for each sensitivity index which can be evaluated by Monte Carlo simulation using various sampling schemes. However, it can be a costly computation, in particular for more demanding simulations such as submarining simulations, as drawing different samples (size N) with n model parameters requires $N2^n$ model evaluations. A computationally efficient method, called M-DRM, has been proposed in [66] to calculate sensitivity indices. Using the M-DRM method, a given complex function can be approximated by a product of low dimensional functions. Combined with the Gaussian quadrature, the computational effort in the calculation of

sensitivity indices is significantly reduced. Sensitivity indices are approximated as:

$$\begin{aligned} S_i &= \frac{V_i}{V_Y} \approx \frac{\theta_i/\rho_i^2 - 1}{(\prod_{k=1}^{n} \theta_k/\rho_k^2) - 1} \\ S_{Ti} &\approx \frac{1 - \rho_i^2/\theta_i}{1 - (\prod_{k=1}^{n} \rho_k^2/\theta_k)} \end{aligned} \tag{4.2}$$

where ρ_i and θ_i are one-dimensional integrals that can be efficiently computed by Gaussian quadrature.

$$\begin{aligned} \rho_i &= \int_{X_i} h(X_i, \mathbb{C}_{-i}) f_i(X_i) dX_i \approx \sum_{j=1}^{N_G} w_j h_j(X_i^{(j)}, \mathbb{C}_{-i}) \\ \theta_i &= \int_{X_i} \left[h(X_i, \mathbb{C}_{-i})\right]^2 f_i(X_i) dX_i \approx \sum_{j=1}^{N_G} w_j [h_j(X_i^{(j)}, \mathbb{C}_{-i})]^2 \end{aligned} \tag{4.3}$$

$f_i(X_i)$ is the distribution function for X_i, $\mathbb{C}_{-i}$ is the mid-point (also called cut-point) vector for random variables where all variables are fixed at their mid points except X_i which varies and $h(X_i, \mathbb{C}_{-i})$ is the corresponding functional evaluation. Two things should be noted when using the M-DRM method. Firstly, since the M-DRM method is based on numerical integration, reaching convergence should be ensured by the number of Gauss points used. Secondly, there is a risk that sensitivity indices calculated by the M-DRM method is locally valid, at the parameter set considered for the mid-point. Therefore, it is crucial to evaluate if the consistent qualitative GSA results are obtainable at different mid-point parameter sets.

The GSA was used at the two study levels as:

- Assessing the material parameter identifiability from different experiments, (**Paper A**).
- Identifying the most important aspect of mechanical properties of adipose tissue in submarining, (**Paper C**.)

5 Summary of Appended Papers

- **Paper A:**
  High variation in mechanical behaviour of adipose tissue particularly during impact, as well as the availability of only few studies for characterising its mechanical properties, have made developing a constitutive model challenging. Calibration experiments have to be coordinated well with the characteristics of the model to ensure that it activates all the material parameters to be identified. Hence, what type of information can be obtained from different experiments which has been addressed in **Paper A**. Several experimental setups have been assessed using Global Sensitivity Analysis as a tool. For each experiment, constitute model parameters were considered as inputs and a measurable integral quantity from the experiment as an output. A high sensitivity index for a model parameter indicates its potential to be identified through parameter identification. It has been found that frequency sweep tests in rheometer setups are suitable for characterising a wide spectrum of viscoelastic behaviour of soft tissue. Another finding is adipose tissue behaviour at high impact loading is influenced by it compressibility. The latter is exemplified by Fig. 5.1 where Poisson's ratio has been identified as a sensitive parameter for high impact loading indentation test.

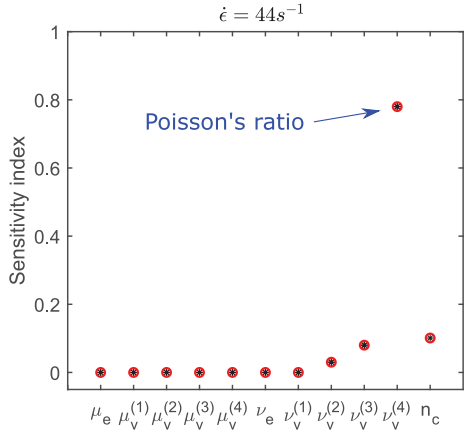

Figure 5.1: *Sensitivity analysis of the indentation test; a high value for the sensitivity index of Poisson's ratio implies its influence on adipose tissue properties at high-impact loading, reproduced from* ***Paper A****.*

- **Paper B:**
  Experimenting on soft tissues with full control and acceptable repeatability of results is practically achievable either for large deformations and low rates or small deformations and high rates. However, here, the behaviour of adipose tissue at large deformation and different loading rates (as in car crashes) is sought. To account for large deformations, a finite strain viscoelasticity model has been used, while for the rate-dependent behaviour, four viscoelastic blocks have been embedded in the model. The wide spectrum of the viscoelastic behaviour of adipose tissue was described by a power-law function in the frequency sweep test, [24]. This feature has been incorporated into the model by imposing a constitutive constraint between the viscoelastic blocks (see also Fig. 2.4). Then, a ramp shear test (at large deformation) was employed to incorporate adipose tissue behaviour at high strain levels. These two tests activate different aspects of the mechanical properties of adipose tissue, thus, a better overall picture of adipose tissue behaviour at different strain rates and strain levels is obtainable than considering the two types of experiments individually.

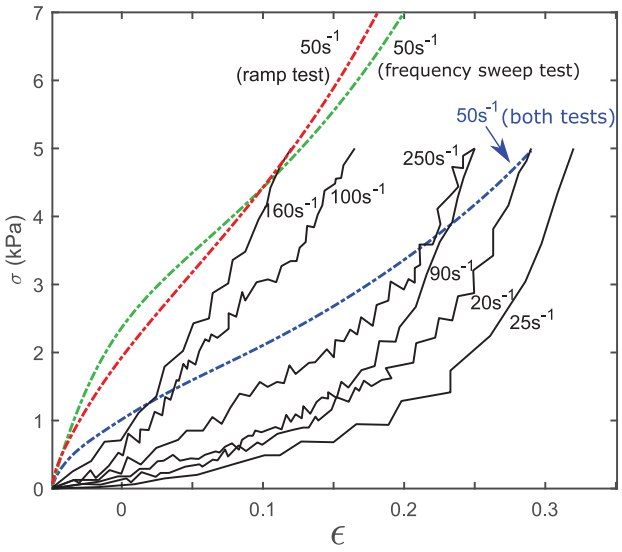

Figure 5.2: *A better prediction of adipose tissue mechanical properties at high strain rates and large deformation is achievable by simultaneously considering a ramp shear test and a frequency sweep test,* ***Paper B****.*

- **Paper C:**
  Submarining, the lap belt sliding over the iliac crest of the pelvic, is a phenomenon that can cause a higher risk of injuries. In this regard, the influence of the mechanical behaviour of adipose tissue can be substantial, particularly for obese occupants having a thick layer of adipose tissue, since the lap belt interacts with the iliac crest of the pelvis through this layer. Therefore, the effect of the developed constitute model for adipose tissue in **Paper B** on lap belt-pelvis interaction has been investigated. To study lap belt-pelvis interaction, the iliac crest of the pelvis and its surrounding parts, namely soft tissue, abdomen and the lap belt has been considered in an FE pelvis submodel. The FE pelvis submodel derives its material model parameters from the SAFER HBM v9 except for the adipose tissue that the newly developed model in **Paper B** is embedded. Submarining was successfully replicated using the new material model. In contrast, submarining could not be captured when the default adipose tissue material model in the THUMS v3 and the GHBMC were used in the FE pelvis submodel. This indicates the significance of a biofidelic model for adipose tissue in submarining prediction. Hence, the main aim of this study, was to identify the most influencing material parameters. Global Sensitivity Analysis was used for this purpose. It has been found that, firstly, the incompressibility condition of adipose tissue is the most influential parameter. This is consistent with the conclusion in **Paper A** identifying the Poisson's ratio as an essential parameter in impact loading. Secondly, the nonlinear elastic and viscoelastic properties are influential due to experiencing large deformation.

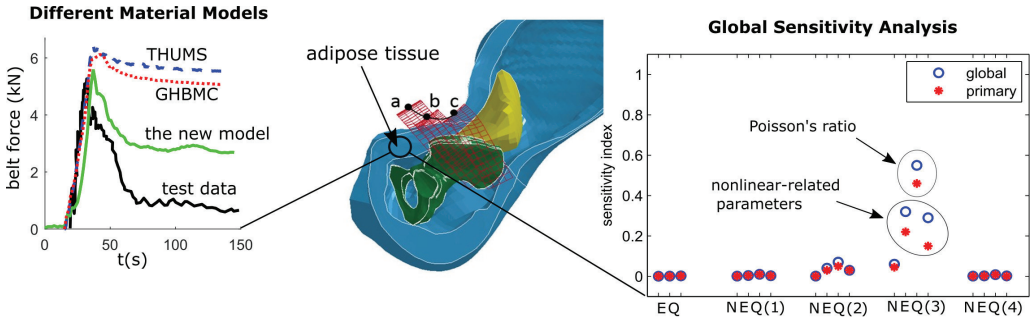

Figure 5.3: *The graphical abstract of* ***Paper C****. Left: The effect of the new material model. Right: Poisson's ratio as the most important material parameter.*

- **Paper D:**
  A closer look at submarining has been paid in this paper. Using the FE pelvis submodel from **Paper C**, several parameters that might influence submarining, as well as the effect of initial lap belt position and obesity on the risk of submarining, have been investigated. Submarining parameters include lap belt angle, lap belt force, belt loading rate, pelvis angle, friction and material properties of adipose tissue. The parameter study was carried out in two steps: Initially, an individual parameter study to find parameters involving higher impact on submarining; Secondly, conducting a further comprehensive study on the parameters identified in the previous step. Belt angle, pelvis angle, Poisson's ratio and belt force were identified as more important parameters than others in the individual parameter study. In the second step, it has been found that the risk of submarining is generally higher for the obese population. The results showed that the interaction effect of important parameters accumulate synergistically for a thicker soft tissue layer, resulting in a higher risk of submarining for obese occupants. The findings of this study can serve as a guideline for the development of biofidelic FEHBMs as well as appropriate restraint system designs to reduce injuries.

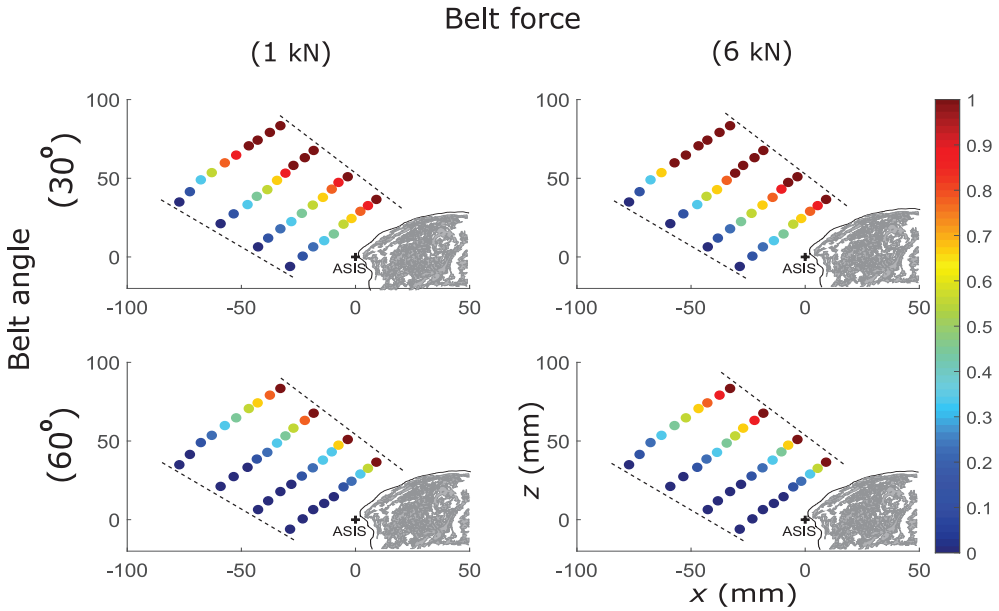

Figure 5.4: *The risk of submarining for different selections of design parameters of belt force and belt angle. Generally, a higher risk of submarining is predicted in all cases for thicker adipose tissue layers,* ***Paper D****.*

6 Conclusion and Future Work

A new biofidelic constitute model for adipose tissue was established, whereby submarining was studied and influencing parameters were identified. The research questions in the beginning of this study was used to conclude the work:

At the Tissue Level:

- Which information can be obtained from different experimental setups used for characterising adipose tissue properties?
  - A wide spectrum of rate-dependent properties can be obtained from frequency sweep tests. Ramp-loading shear tests can characterise nonlinear shear properties at a certain rate. Depending on the loading rate, both shear and bulk stiffness can be activated in unconfined compression tests and indentation tests. Although, at high loading rates, bulk stiffness dominates the response and the tissue behaviour is highly influenced by its incompressibility.
- What is a reliable parameter identification for the adipose tissue constitutive model, considering the high variation in the adipose tissue behaviour at large deformation and high strain rates?
  - Considering frequency sweep tests along with a ramp-loading shear test seems a good combination to identify rate-dependent and nonlinear features of adipose tissue. Unfortunately, incompressibility of adipose tissue cannot be identified from these tests though it is an important parameter at high loading rates.
- What is a suitable constitutive model to predict adipose tissue behaviour in vehicle crash situations?
  - A constitute model that incorporates a wide range of strain rates as well as nonlinear features associated with elastic (hardening) and viscoelastic (softening) behaviours.

At the Human Body Level:

- What is the advantage of the new constitutive model to submarining prediction compared to the current material models in FEHBMs for adipose tissue?
  - It is able to successfully predict submarining observed in physical tests while current models are over-stiff preventing the belt sliding over the pelvis.

- What features of adipose tissue influence the submarining behaviour the most?
  - The incompressibility level of adipose tissue is the most important followed by the nonlinear properties.
- What other parameters, including vehicle-design and occupant parameters influence the mechanism of submarining? How do obesity and initial lap belt position influence?
  - Belt angle and pelvis angle have been identified as important safety design parameters. The interaction effect of these parameters accumulate synergistically for a thicker soft tissue layer, resulting in a higher risk of submarining for obese occupants.

The incompressibility of adipose tissue, or Poisson's ratio, has been found to represent an important parameter in the mechanical behaviour of adipose tissue during impact, e.g., in submarining. However, to date a thorough experimental investigation on this property for adipose tissue has not been carried out. This is a critical question for future research at the tissue level. On the human body level, an interesting topic for study would include considering the multi-layer structure of the flesh tissue in the front of ASIS in order to clarify the effect the muscle layer has on the submarining mechanism.

Bibliography

[1] Petridou, E. T., and Antonopoulos, C. N., 2017. "Injury epidemiology". In *International Encyclopedia of Public Health (Second Edition)*, S. R. Quah, ed., second edition ed. Academic Press, Oxford, pp. 258 – 274.

[2] Rice, T. M., and Zhu, M., 2013. "Driver obesity and the risk of fatal injury during traffic collisions". *Emerg Med J*, pp. emermed–2012.

[3] Rupp, J. D., Flannagan, C. A., Leslie, A. J., Hoff, C. N., Reed, M. P., and Cunningham, R. M., 2013. "Effects of bmi on the risk and frequency of ais 3+ injuries in motor-vehicle crashes". *Obesity,* **21**(1).

[4] Reed, M. P., Ebert, S. M., and Hallman, J. J., 2013. "Effects of driver characteristics on seat belt fit". *Stapp Car Crash Journal,* **57**, pp. 43–57.

[5] Jones, M. L., Ebert, S., Hu, J., and Reed, M. P., 2017. "Effects of high levels of obesity on lap and shoulder belt paths". *International Research Council on Biomechanics of Injury (IRCOBI)*, pp. 13–15.

[6] Reed, M. P., Ebert-Hamilton, S. M., and Rupp, J. D., 2012. "Effects of obesity on seat belt fit". *Traffic injury prevention,* **13**(4), pp. 364–372.

[7] Forman, J., Lopez-Valdes, F. J., Lessley, D., Kindig, M., Kent, R., and Bostrom, O., 2009. "The effect of obesity on the restraint of automobile occupants". In Annals of Advances in Automotive Medicine/Annual Scientific Conference, Vol. 53, Association for the Advancement of Automotive Medicine, p. 25.

[8] Uriot, J., Baudrit, P., Potier, P., Trosseille, X., Petit, P., Guillemot, H., Guérin, L., and Vallancien, G., 2006. "Investigations on the belt-to-pelvis interaction in case of submarining". *Stapp Car Crash Journal,* **50**, pp. 53–73.

[9] McMurry, T. L., Poplin, G. S., Shaw, G., and Panzer, M. B., 2018. "Crash safety concerns for out-of-position occupant postures: A look toward safety in highly automated vehicles". *Traffic injury prevention,* **19**(6), pp. 582–587.

[10] Dissanaike, S., Kaufman, R., Mack, C. D., Mock, C., and Bulger, E., 2008. "The effect of reclined seats on mortality in motor vehicle collisions". *Journal of Trauma and Acute Care Surgery,* **64**(3), pp. 614–619.

[11] Thorbole, C. K., 2015. "Dangers of seatback recline in a moving vehicle: how seatback recline increases the injury severity and shifts injury pattern". In ASME

2015 International Mechanical Engineering Congress and Exposition, American Society of Mechanical Engineers Digital Collection.

[12] Richard, O., Uriot, J., Trosseille, X., and Sokolowski, M., 2015. "Occupant restraint optimisation in frontal crash to mitigate the risk of submarining in out-of-position situation". In Proceedings of IRCOBI Conference.

[13] Mendoza-Vazquez, M., Davidsson, J., and Brolin, K., 2015. "Construction and evaluation of thoracic injury risk curves for a finite element human body model in frontal car crashes". *Accident Analysis & Prevention,* **85**, pp. 73–82.

[14] Östh, J., Mendoza-Vazquez, M., Sato, F., Svensson, M. Y., Linder, A., and Brolin, K., 2017. "A female head–neck model for rear impact simulations". *Journal of Biomechanics,* **51**, pp. 49 – 56.

[15] Mendoza-Vazquez, M., Brolin, K., Davidsson, J., and Wismans, J., 2013. "Human rib response to different restraint systems in frontal impacts: a study using a human body model". *International journal of crashworthiness,* **18**(5), pp. 516–529.

[16] Östh, J., Brolin, K., Svensson, M. Y., and Linder, A., 2016. "A female ligamentous cervical spine finite element model validated for physiological loads". *Journal of biomechanical engineering,* **138**(6).

[17] Iwamoto, M., Kisanuki, Y., Watanabe, I., Furusu, K., Miki, K., and Hasegawa, J., 2002. "Development of a finite element model of the total human model for safety (THUMS) and application to injury reconstruction". *Proceedings of the 2002 International Research Council on Biomechanics of Injury, Munich, Germany*, pp. 31–42.

[18] Iwamoto, M., Nakahira, Y., and Kimpara, H., 2015. "Development and validation of the total human model for safety (THUMS) toward further understanding of occupant injury mechanisms in precrash and during crash". *Traffic Injury Prevention,* **16**(sup1), pp. S36–S48. PMID: 26027974.

[19] Shin, J., Yue, N., and Untaroiu, C. D., 2012. "A finite element model of the foot and ankle for automotive impact applications". *Annals of biomedical engineering,* **40**(12), pp. 2519–2531.

[20] Gayzik, F. S., Moreno, D. P., Vavalle, N. A., Rhyne, A. C., and Stitzel, J. D., 2011. "Development of the global human body models consortium mid-sized male full body model". In International Workshop on Human Subjects for Biomechanical Research, Vol. 39, National Highway Traffic Safety Administration.

[21] Naseri, H., Johansson, H., and Iraeus, J., 2020. "The effect of adipose tissue material properties on the lap belt-pelvis interaction: A global sensitivity analysis". *Accepted for application in the journal of mechanical behavior of biomedical materials*.

[22] Comley, K., and Fleck, N., 2012. "The compressive response of porcine adipose tissue from low to high strain rate". *International Journal of Impact Engineering,* **46**, pp. 1 – 10.

[23] Comley, K., and Fleck, N. A., 2010. "A micromechanical model for the young's modulus of adipose tissue". *International Journal of Solids and Structures,* **47**(21), pp. 2982–2990.

[24] Geerligs, M., Peters, G. W., Ackermans, P. A., Oomens, C. W., and Baaijens, F., 2008. "Linear viscoelastic behavior of subcutaneous adipose tissue". *Biorheology,* **45**(6), pp. 677–688.

[25] Geerligs, M., Peters, G. W., Ackermans, P. A., Oomens, C. W., and Baaijens, F. P., 2010. "Does subcutaneous adipose tissue behave as an (anti-) thixotropic material?". *Journal of biomechanics,* **43**(6), pp. 1153–1159.

[26] Gefen, A., and Haberman, E., 2007. "Viscoelastic properties of ovine adipose tissue covering the gluteus muscles". *Journal of biomechanical engineering,* **129**(6), pp. 924–930.

[27] Fuster, J. J., Ouchi, N., Gokce, N., and Walsh, K., 2016. "Obesity-induced changes in adipose tissue microenvironment and their impact on cardiovascular disease.". *Circulation research,* **118 11**, pp. 1786–807.

[28] Sommer, G., Eder, M., Kovacs, L., Pathak, H., Bonitz, L., Mueller, C., Regitnig, P., and Holzapfel, G. A., 2013. "Multiaxial mechanical properties and constitutive modeling of human adipose tissue: a basis for preoperative simulations in plastic and reconstructive surgery". *Acta biomaterialia,* **9**(11), pp. 9036–9048.

[29] Guilak, F., and Mow, V. C., 2000. "The mechanical environment of the chondrocyte: a biphasic finite element model of cell–matrix interactions in articular cartilage". *Journal of biomechanics,* **33**(12), pp. 1663–1673.

[30] Miller, K., Taylor, Z., and Nowinski, W. L., 2005. "Towards computing brain deformations for diagnosis, prognosis and neurosurgical simulation". *Journal of Mechanics in Medicine and Biology,* **5**(01), pp. 105–121.

[31] Dutta-Roy, T., Wittek, A., and Miller, K., 2008. "Biomechanical modelling of normal pressure hydrocephalus". *Journal of biomechanics,* **41**(10), pp. 2263–2271.

[32] Tanner, R. I., 2000. *Engineering rheology*, Vol. 52. OUP Oxford.

[33] Holzapfel, G. A., and Gasser, T. C., 2001. "A viscoelastic model for fiber-reinforced composites at finite strains: Continuum basis, computational aspects and applications". *Computer methods in applied mechanics and engineering,* **190**(34), pp. 4379–4403.

[34] Laksari, K., Shafieian, M., and Darvish, K., 2012. "Constitutive model for brain tissue under finite compression". *Journal of biomechanics,* **45**(4), pp. 642–646.

[35] Rashid, B., Destrade, M., and Gilchrist, M. D., 2013. "Mechanical characterization of brain tissue in simple shear at dynamic strain rates". *Journal of the mechanical behavior of biomedical materials,* **28**, pp. 71–85.

[36] Miller, K., and Chinzei, K., 2002. "Mechanical properties of brain tissue in tension". *Journal of biomechanics,* **35**(4), pp. 483–490.

[37] Reese, S., and Govindjee, S., 1998. "A theory of finite viscoelasticity and numerical aspects". *International journal of solids and structures,* **35**(26-27), pp. 3455–3482.

[38] Hrapko, M., Van Dommelen, J., Peters, G., and Wismans, J., 2006. "The mechanical behaviour of brain tissue: large strain response and constitutive modelling". *Biorheology,* **43**(5), pp. 623–636.

[39] Brands, D., Peters, G., and Bovendeerd, P., 2004. "Design and numerical implementation of a 3-d non-linear viscoelastic constitutive model for brain tissue during impact". *Journal of biomechanics,* **37**(1), pp. 127–134.

[40] Bathe, K.-J., 2006. *Finite element procedures*. Klaus-Jurgen Bathe.

[41] Bathe, K.-J., and Baig, M. M. I., 2005. "On a composite implicit time integration procedure for nonlinear dynamics". *Computers & Structures,* **83**(31), pp. 2513–2524.

[42] Bathe, K.-J., and Noh, G., 2012. "Insight into an implicit time integration scheme for structural dynamics". *Computers & Structures,* **98**, pp. 1–6.

[43] *Guide for verification and validation in computational solid mechanics*. ASME Committee (PT60) on Verification and Validation in Computational Solid Mechanics, 2006.

[44] *AIAA Guide for the verification and validation of computational fluid dynamics simulations*. No. Rep. G-077-1998e. American Institute of Aeronautics and Astronautics, 1998.

[45] Oberkampf, W. L., Trucano, T. G., and Hirsch, C., 2004. "Verification, validation, and predictive capability in computational engineering and physics". *Appl. Mech. Rev.,* **57**(5), pp. 345–384.

[46] Babuska, I., and Oden, J. T., 2004. "Verification and validation in computational engineering and science: basic concepts". *Computer methods in applied mechanics and engineering,* **193**(36), pp. 4057–4066.

[47] Naseri, H., Johansson, H., and Brolin, K., 2016. "Modeling the mechanical behavior of adipose tissue". In 29th Nordic Seminar on Computational Mechanics, NSCM-29, R. Larsson (Ed.), p. 4 pages.

[48] Patel, P. N., Smith, C. K., and Patrick Jr, C. W., 2005. "Rheological and recovery properties of poly (ethylene glycol) diacrylate hydrogels and human adipose tissue". *Journal of Biomedical Materials Research Part A: An Official Journal of The Society for Biomaterials, The Japanese Society for Biomaterials, and The Australian Society for Biomaterials and the Korean Society for Biomaterials,* **73**(3), pp. 313–319.

[49] Kim, T., Park, G., Montesinos, S., Subit, D., Bolton, J., Overby, B., Forman, J., Crandall, J., and Kim, H., 2015. "Abdominal characterization test under lap belt loading". *24th International Technical Conference on the Enhanced Safety of Vehicles (ESV), National Highway Traffic Safety Administration, Gothenburg, Sweden*, pp. 15–0312.

[50] Iraeus, J., and Pipkorn, B., 2019. "Development and validation of a generic finite element ribcage to be used for strain-based fracture prediction". *Proceedings of the 2019 International Research Council on Biomechanics of Injury, Florence, Italy*, pp. 193–210.

[51] Pipkorn, B., Iraeus, J., Björklund, M., Bunketorp, O., and Jakobsson, L., 2019. "Multi-scale validation of a rib fracture prediction method for human body models". *Proceedings of the 2019 International Research Council on Biomechanics of Injury, Florence, Italy*, pp. 175–192.

[52] Steffan, H., Hofinger, M., Parenteau, C., Shah, M., Webber, J., Darok, M., and Leinzinger, P., 2002. "Abdominal responses to dynamically lap belt loading". In Proceeding of IRCOBI Conference. Munich, Germany.

[53] Luet, C., Trosseille, X., Drazétic, P., Potier, P., and Vallancien, G., 2012. "Kinematics and dynamics of the pelvis in the process of submarining using PMHS sled tests". *Stapp Car Crash Journal,* **56**, pp. 411–442.

[54] Ellis, B. J., Debski, R. E., Moore, S. M., McMahon, P. J., and Weiss, J. A., 2007. "Methodology and sensitivity studies for finite element modeling of the inferior glenohumeral ligament complex". *Journal of biomechanics,* **40**(3), pp. 603–612.

[55] Naseri, H., Johansson, H., and Brolin, K., 2018. "A nonlinear viscoelastic model for adipose tissue representing tissue response at a wide range of strain rates and high strain levels". *Journal of biomechanical engineering,* **140**(4), p. 041009.

[56] Boulay, C., Tardieu, C., Hecquet, J., Benaim, C., Mouilleseaux, B., Marty, C., Prat-Pradal, D., Legaye, J., Duval-Beaupère, G., and Pélissier, J., 2006. "Sagittal alignment of spine and pelvis regulated by pelvic incidence: standard values and prediction of lordosis". *European Spine Journal,* **15**(4), Apr, pp. 415–422.

[57] Saltelli, A., Tarantola, S., Campolongo, F., and Ratto, M., 2004. *Sensitivity analysis in practice: a guide to assessing scientific models.* John Wiley & Sons.

[58] Naseri, H., and Johansson, H., 2018. "A priori assessment of adipose tissue mechanical testing by global sensitivity analysis". *Journal of biomechanical engineering,* **140**(5), p. 051008.

[59] A.E. Anderson, C.L. Peters, B. T., and J.A.Weiss, 2005. "Subject-specific finite element model of the pelvis: development, validation and sensitivity studies". *Journal of biomechanical engineering,* **127**(3), p. 364–373.

[60] Phatak, N. S., Sun, Q., Kim, S.-E., Parker, D. L., Sanders, R. K., Veress, A. I., Ellis, B. J., and Weiss, J. A., 2007. "Noninvasive determination of ligament strain with deformable image registration". *Annals of biomedical engineering,* **35**(7), pp. 1175–1187.

[61] Donahue, T. L. H., Hull, M., Rashid, M. M., and Jacobs, C. R., 2003. "How the stiffness of meniscal attachments and meniscal material properties affect tibio-femoral contact pressure computed using a validated finite element model of the human knee joint". *Journal of biomechanics,* **36**(1), pp. 19–34.

[62] French, S., 2003. "Modelling, making inferences and making decisions: the roles of sensitivity analysis". *Top,* **11**(2), pp. 229–251.

[63] Sobol', I. M., 1990. "On sensitivity estimation for nonlinear mathematical models". *Matematicheskoe modelirovanie,* **2**(1), pp. 112–118.

[64] Saltelli, A., and Sobol, I. M., 1995. "About the use of rank transformation in sensitivity analysis of model output". *Reliability Engineering & System Safety,* **50**(3), pp. 225–239.

[65] Homma, T., and Saltelli, A., 1996. "Importance measures in global sensitivity analysis of nonlinear models". *Reliability Engineering & System Safety,* **52**(1), pp. 1–17.

[66] Zhang, X., and Pandey, M. D., 2014. "An effective approximation for variance-based global sensitivity analysis". *Reliability Engineering & System Safety,* **121**, pp. 164–174.